A Quantitative Model of Ultraviolet Matrix-assisted Laser Desorption/Ionization including Analyte Ion Generation

Richard Knochenmuss

Author's final submitted manuscript
Published as Anal. Chem., vol. 75, pp. 2199-2207 (2003)
DOI: 10.1021/ac034032r
URL: http://pubs.acs.org/doi/abs/10.1021/ac034032r

Abstract

A quantitative model of ionization in ultraviolet matrix-assisted laser desorption/ionization (R. Knochenmuss, J. Mass Spectrom. 37, 867 (2002)) is extended to include secondary ion-molecule reactions. Matrix-to-analyte charge transfer reaction kinetics are described by a hard-sphere Arrhenius expression. The activation energy is derived from the reaction exoergicity using a nonlinear free energy relationship. The approach is applied to the specific case of proton transfer reactions. With no adjustable parameters, the model correctly predicts the existence and characteristics of the matrix and analyte suppression effects, the shapes of the 2-pulse time-delayed yield curves, as well as the dependence of analyte yields on laser fluence, molecular weight, relative concentrations and reaction exoergicity.

Introduction

The first quantitatively successful model for MALDI (Matrix Assisted Laser Desorption/Ionization) with ultraviolet (UV) laser excitation was recently presented.[1] That model was concerned with primary ionization in a MALDI sample containing only matrix. The key microscopic processes involved are energy pooling between pairs of neighboring or colliding excited molecules. A molecular beam model of the plume expansion was found to be necessary to account for decreasing collision rates as the sample expands into the vacuum. Following determination of the pooling parameters using fluorescence quenching[2] and time-delayed 2-pulse data,[3] the model was able to reproduce a range of MALDI phenomena: The existence of a fluence threshold, in the correct fluence range; a fluence rather than irradiance dependence of the threshold, and a weak irradiance dependence above threshold; the absorption cross section dependence of the threshold; the magnitude of the ion yield; plume temperatures; plume expansion velocities; the spot size effect.

While the model describing only matrix ion generation was quite successful, it is of limited practical use without analyte. That limitation is removed in the present work. As proposed in detail by Knochenmuss et al.,[4] and supported by more recent evidence,[5,6] analyte ionization in MALDI is often thermodynamically controlled, as the result of secondary ion-molecule reactions in the plume. During or shortly after the laser pulse, primary ions are generated. In the ensuing desorption plume expansion, ion-molecule reactions convert the primary ions to the most favorable secondary products, which are observed at the detector.

Among the more direct indications for this picture are the remarkable MALDI phenomena known as the matrix suppression[7,8] and analyte suppression effects.[4] As will be shown in detail below, the matrix suppression effect (MSE) occurs when enough analyte is present in the sample to react with all the primary ions. Ideal mass spectra are the result: only analyte signal, with no confusing matrix ions. A particularly remarkable aspect of the MSE is that a single type of analyte ion (e.g. protonated) can suppress all matrix ions, be they protonated, cationized or radicals. Multiple suppression is evidence of extensive matrix-matrix ion-molecule reactions in the plume.[4]

Analytes can also strongly influence each other, if concentrations are high enough. Analogous to the MSE it was shown that an analyte suppression effect (ASE) exists, and that dissimilar analyte ions can suppress each other (e.g. protonated and sodiated).[4] Both the MSE and ASE are thermodynamically predictable. They occur if

there is sufficient driving force for the ion-molecule reactions leading to the observed (suppressing) ion.

Matrix-analyte secondary reactions are integrated into the model of ref. 1 by adding the appropriate equations to the matrix-only system, which is numerically solved. Within the thermodynamic picture of the plume, an Arrhenius expression is appropriate for the secondary reaction rates. A straightforward hard sphere prefactor is used, and the activation energy is calculated using an established nonlinear free energy relationship. In addition, the high density early phase of the expansion requires an excluded volume correction for large analytes. These additions to the theory do not depend on fitted parameters, yet are able to explain and reproduce key features of MALDI, particularly 2-pulse experiments, and the characteristics of suppression effects.

Continuum Model including Analyte

Analyte Ion Generation Pathways

Analyte is assumed here to become ionized only via secondary reactions. Two other potential analyte ion generation pathways are neglected: preformed ions and direct laser generation.[5] Preformed ions may exist in the solid sample prior to laser excitation,[9,10] although they are also expected to be strongly associated with counterions. As a result of the latter, "liberation" of preformed ions may be an energetic process that is too slow at typical plume temperatures to make a major contribution to the analyte ion yield. A similar conclusion was reached for matrix disproportionation reactions, which are thermodynamically closely related.[11,12]

Direct UV laser ionization of analytes is less straightforward. While most common analytes do not strongly absorb the laser, it has been recently shown that analyte-matrix interactions can lead to lowering of ionization potentials of appropriately coordinated matrix.[13-15] Clusters of matrix with analyte that are 2-photon ionized by this pathway have been calculated to undergo barrierless secondary intra-cluster proton transfer to analyte. Strictly speaking this is again a case of primary matrix ionization followed by reaction with neutral analyte, but the primary step is enabled by analyte, blurring the distinction between primary and secondary reactions.

Direct UV analyte ionization needs to be further studied, but it cannot be active for all analytes and matrices, since it depends on special matrix-analyte coordination. Also, analytes are nearly always present in small amounts compared to matrix, so the ion current will be dominated by matrix-only primary steps. Consequently the fraction of

analyte which might be directly ionized is expected to be much smaller than that ionized by reaction with primary matrix ions. For example, if the analyte is present in 10^{-4} mole ratio to the matrix, a direct ionization mechanism would need to be roughly 10^4 times more efficient than reaction with matrix primary ions, just to reach equal ionization efficiency. Such a high efficiency currently appears unlikely.

Based on these considerations, the reaction model assumed here is that primary matrix ions are generated via the same mechanisms as when analyte is absent. Subsequently these ions react with analyte neutrals:

$$M^+ + A \rightarrow M + A^+$$

Matrix and analyte ions are denoted here as M^+ and A^+, but may be of either polarity and any type: radical cations, protonated, sodiated, deprotonated, etc. The reaction is assumed to be reversible, since it may be near thermoneutral.

Implementation of the Secondary Analyte Reaction Model

The rate equation approach[1,16-18] treats the MALDI sample as a continuous medium for which local temperature is well defined. These approximations have proven highly successful, but may in the future need refinement by comparison to molecular dynamics[19-22] to account for non-equilibrium effects, particularly at short times.

The recent matrix-only model[1] includes rate equations for the matrix ground electronic state (S_0), the first excited singlet state (S_1), a higher excited singlet state (S_n, at twice the photon energy, but below the ionization potential), the ion state, and the matrix internal energy (which is assumed to yield a local temperature). Excitation energy pooling is accounted for by terms involving the product of two excited states.

Reaction of a single analyte with primary matrix ions is included by adding new equations for the reactions:

$$M^+ + A \rightarrow M + A^+$$

$$d[A]/dt = -k_{MA}[M^+][A] + k_{AM}[M][A^+]$$

$$d[A^+]/dt = k_{MA}[M^+][A] - k_{AM}[M][A^+]$$

Mass balance requires that corresponding terms are also added to the equations for M and M^+. Again, the ionized analyte is denoted as A^+ for convenience, although the type of ion is arbitrary. As in ref. 1, both the forward charge transfer reaction rate, k_{MA}, and the reverse rate, k_{AM}, are scaled by the pressure ratio of the expanding plume to account for decreasing bimolecular collision rates after desorption starts.

$$k_{\mathrm{MA}} = A\mathrm{e}^{-\mathrm{EA}/kT}$$

$$k_{\mathrm{AM}} = A\mathrm{e}^{-(\mathrm{EA}+\Delta G)/kT}$$

The rates k_{MA} and k_{AM} are assumed to be of Arrhenius form:
The forward reaction is taken to be exoergic with activation energy EA, so the reverse reaction activation energy is larger by the exoergicity. Within the hard sphere approximation, the prefactor is the collision rate:

$$A = \pi(D_{\mathrm{M}} + D_{\mathrm{A}})^2 F(1-F) n \sqrt{V_{\mathrm{M}}{}^2 + V_{\mathrm{A}}{}^2}$$

Where the D_i are the molecular radii, F is the mole fraction of analyte in the sample, and n is the total number density of all matrix and analyte species. The V_i are the sound speeds of matrix or analyte:

$$V_{\mathrm{sound}} = \sqrt{\gamma RT/(\mathrm{MW})}$$

$$\gamma = C_{\mathrm{P}}/C_{\mathrm{V}}$$

Where MW is the molecular weight and g is the heat capacity ratio of the expanding plume. Without steric correction factors it is often the case that the hard sphere prefactor is somewhat too large. It is retained here without modification because general steric prefactors are not known for MALDI matrices and analytes.

The molecular diameters were taken from a fit to the data of figure 3 of Valentine, et al.[23] These data for singly charged ion mobility cross sections (in $Å^2$) were well fit by the equation:

$$\sigma = 2.38(\mathrm{MW})^{2/3}$$

from which the collision radii (cm) follow:

$$D = 7.58\times10^{-9}(\mathrm{MW})^{1/3}$$

This expression presumably slightly overestimates radii for the neutral reaction partner, but was not found to be significantly different from radii estimated from solid densities.

The MALDI plume begins at very high density, as the solid sample disintegrates. The hard-sphere picture is therefore not entirely valid at early times, since it is derived for gas-phase reactions in which molecular excluded volumes are insignificant. Therefore one of the most important corrections necessary in the MALDI case is for the relative sizes of the matrix and analyte. Analyte molecular weights can be orders of magnitude larger than those of the matrix in which they are imbedded. Clearly a large analyte will have a higher probability of collision with neighboring primary matrix ions at early times than a small analyte. A surface area correction factor was therefore included in the rate constant prefactor:

$$1+[(D_A/D_M)^2 - 1]P/Po$$

At the start of desorption the pressure ratio, P/P_o, is unity,[1] and the collision rate is scaled by the relative surface areas of analyte and matrix. At long times, when the hard sphere prefactor is most valid, P/P_o becomes negligible and the correction factor approaches one, having no effect.

Since no completely general expression for activation energies exists, one was chosen which has been found to be successful for a number of gas-phase proton transfer reactions. The Agmon-Levine relationship is a nonlinear function of the free energy:[24,25]

$$\mathrm{EA} = \Delta G - \lambda \ln\left(\frac{1}{1 + \mathrm{e}^{-\Delta G/\lambda}}\right)$$

Where the ΔG is the reaction exoergicity, and the factor l is related to the activation barrier at thermoneutrality: $EA(\Delta G=0)=\lambda \ln(2)$. Typical values of λ for proton transfer reactions are 14-19 kJ/mol.[24] For this work a value of 15 was chosen, from studies of gas-phase proton transfer reactions of MALDI matrices.[11] This choice is seldom critical, the reaction exoergicity has a much larger effect, as seen in Fig. 1. If the reaction is strongly favorable, its rate is collisionally limited. Less favorable reactions show an increasing lambda dependence, which nevertheless becomes highly significant only at the lowest ΔG values.

FIG 1 EA vs ΔG, Lambda

Multiple Analytes

Having developed a method to treat matrix/analyte ion-molecule reactions, it is straightforward to extend this to more analytes. Each analyte obviously undergoes reaction with matrix, but they can also react with each other. The corresponding rate equations are analogous to those for reaction of a single analyte with matrix above. The same expressions are used for activation energies and plume collision rate scaling.

Numerical Integration

The primary ionization parameters were as reported in Ref. 1. The rate equations were numerically integrated using double precision 5th order Runge-Kutta methods, as included in the Igor data analysis package (WaveMetrics Inc., Lake Oswego, OR, USA). The number of time points was increased until no further change in the result was observed. A large number of time steps was particularly important when using short laser pulses. The depth integration was carried out until the laser was attenuated to <5% of its initial value. The number of depth slices was typically 100.

Results and Discussion

Model Results and Reaction Time Scales

As intuitively expected, Fig, 2 shows that reaction of matrix ions with neutral analyte begins as soon as significant amount of matrix ions are present. Secondary reactions are therefore of the same general time scale as matrix ion generation. Since the plume becomes dilute relatively rapidly, the bulk of reaction is over in about 10 ns for the parameters of Fig. 2. The overlapping nature of primary and secondary reactions minimizes analyte peak broadening in time-of-flight experiments. A significantly slower reaction, for example due to a less vigorous plume expansion, would not be consistent with experimentally observed time-of-flight resolution. Slower further reaction occurs downstream, to and past the right edge of Fig. 2, as observed in energy deficit measurements by Kinsel et al.[26] This picture does not exclude release of ions by evaporation of matrix-analyte clusters,[27,28] which are not modeled here, and not believed to be major contributors.

FIG 2 example calculation

Effect of Reaction Exoergicity, Molecular Weight and Laser Fluence

As known experimentally and predicted by the earlier matrix-only model, total ion current increases with increasing laser fluence. To more clearly understand the effects of analyte on the model, and to facilitate comparison with experiment, it is therefore often more useful to plot the matrix/analyte (M/A) ion ratio rather than absolute ion signals.

FIG 3 M/A vs DG

Figure 3 shows the M/A ion yield ratio vs. the exoergicity of the analyte ion generation reaction, for one analyte. It is notable that the curve is flat over a wide DG range, for a wide range of parameters. Only above about -30 kJ/mol does analyte signal begin to decrease significantly due to incomplete reaction. The shapes of the curves in Fig. 3 explain much of the wide utility of MALDI. The reaction of matrix ions with neutral analyte need only be moderately favorable to yield extensive reaction and a good analyte signal.

Some other important trends are visible in Fig. 3. More analyte means more matrix ions are consumed, and the M/A ratio drops, as seen from traces (a) and (b). Increasing laser fluence increases the amount of primary ions available, and so the M/A ratio, compare (b) and (c). Also very important is the effect of analyte molecular

weight. Curve (d) shows how a larger analyte more efficiently consumes primary matrix ions due to a higher reaction cross section, leading to a low M/A ratio. This effect will be discussed in more detail below. In this case, for $\Delta G<-40$ kJ/mol, full matrix suppression is achieved, the M/A ratio is zero. It should also not be noted that the results presented here do not take into account the usual steep drop in detection efficiency for larger ions, which will significantly affect all nonzero M/A ratios.[29-31]

The horizontal axis of Fig. 3 covers an experimentally important range. The gas-phase basicities of proteins and peptides[32-36] are generally significantly higher than those of common matrices,[12,37-39] so the reaction exoergicities expected are on the left side of Fig. 3. Analyte ion generation is facile, and such analytes are known to be readily observed with MALDI, with high sensitivity. In contrast, metal cation affinities are as much as an order of magnitude lower (Na^+: 150-170 kJ/mol, K^+: order of 50 kJ/mol) with correspondingly smaller differences between matrix and analyte.[40-43] MALDI experiments where cationization is the primary route to analyte ions (e.g. many synthetic polymers) are therefore working on the right half of Fig. 3, and extensive analyte ion production may be difficult to achieve. This is in accord with the general observation that many synthetic polymers, especially those with few functional groups, are relatively difficult to analyze with MALDI.[44]

Nanosecond 2-pulse MALDI Experiments

Fig 4 ako2p

The time-delayed 2-pulse effect[3,8] was both a key test for and a means to determine parameters in the original matrix-only rate equation MALDI model.[1] Two sub-threshold pulses are combined with a time delay to give a strong MALDI signal. This remarkable phenomenon has recently also been demonstrated for analyte ions by Moskovets and Vertes.[45] The 337 nm, 3 ns nitrogen laser pulsewidth limited resolution compared to the 30 ps matrix-only experiments, but very significant differences were nevertheless found between matrices. These data are particularly useful since they are sensitive to plume and matrix-analyte reaction dynamics. Both early processes in the high density region and later "gas-phase" reactions contribute to the curves, making them a difficult test of the model.

As seen in Fig. 4, the model is in quantitative agreement with the measured data for substance P in DHB matrix. Considering only the time points of Moskovets and Vertes, an exponential curve is obtained. When additional points are calculated at

early times, it becomes apparent that non-exponential structure should be observable, due to temporal overlap of the two pulses. Excepting the laser wavelength, this result was achieved with the matrix ionization parameters of ref. 1, no modification or fitting was performed. The only analyte parameter that was *a priori* unknown and hence not fixed was the reaction ΔG. This was taken to be typical for peptides, -150 kJ/mol.

Also shown in Fig. 4 are two-pulse data of Moskovets and Vertes for a-cyano-4-hydroxycinnamic acid matrix. This curve has the most extreme non-exponential shape they observed. While the not all necessary physical properties are known for this matrix, by adjusting parameters such as sublimation temperature, excited state lifetime, and degree of decomposition (but without fitting) the model is capable of generating appropriate curves. The characteristics of the plume and hence the 2-pulse curve are also dependent on non-matrix factors such as the laser spot size. This result shows that the model may be applicable to matrices other than DHB with only minor adaptation of parameters, but is not intended to imply that the model is universal.

Ion Signal vs. Analyte Concentration (Matrix Suppression Effect)

FIG 5 M/A vs conc of A

Figure 5 shows the calculated dependence of the M/A ion ratio on analyte concentration in the sample. The ΔG is typical of peptides, -150 kJ/mol. Over a range of analyte molecular weights a qualitatively similar curve is observed. From right to left (increasing analyte concentration) there is a nonlinear drop in the M/A signal ratio until finally no more matrix ions are observed. In other words the matrix suppression effect (MSE) is predicted. When sufficient analyte is present in the sample, only analyte ions are observed, and no matrix ions. Experimentally, a nonlinear concentration dependence is also observed, but with more structure than in Fig. 5.[7] In particular, a plateau followed by a step to zero M/A is often found.

The [M]/[A] ratio in the sample at which the M/A ion ratio drops to zero is strongly dependent on the analyte molecular weight (MW). This effect is also observed experimentally.[7] For molecular weights near 1000 Da, the concentration ratio for MSE was found to be in the range 10-100, the calculated value is in good agreement at 100. For large molecules, limited data is available, but experiments do show a significant increase in the suppression concentration threshold. For 10 kDa a [M]/[A]

value of 1000-1500 can be extrapolated. The model predicts a weaker MW dependence, the 10 kDa MSE threshold is only 200.

Apparently the calculated large-molecule reaction rates are not as high as they should be. The molecular weight effect is due to the hard-sphere prefactor and the spherical surface area scaling at early expansion times. Since a sphere is likely an increasingly poor approximation of larger molecules, it is perhaps to be expected that the model gives a less dramatic molecular weight dependence than found experimentally.

It is important to note that the matrix suppression effect is easy to understand in the present model. When sufficient neutral analyte is present to react with all matrix ions, the reaction is significantly exoergic, and the plume is dense, the reaction runs to completion. It should also be noted that other qualitative MALDI models cannot account for the MSE. For example, in a model based entirely on preformed ions, there is no means for analyte to influence matrix ion yield or vice versa.[9] Similarly, in a model based on reaction of analyte with matrix in solid clusters (and subsequent evaporation),[27,28] matrix ions generated outside clusters must always be observed and at most a weak analyte concentration effect appears. The cluster model of matrix suppression also requires that there are in every case fewer ions in every cluster than analyte molecules, which is implausible. Finally, and most conclusively, no model excluding secondary reactions has been proposed which can explain the suppression of all types of matrix ion by one type of analyte ion (for example M^+, MH^+ and MNa^+ by AH^+ or ANa^+).

FIG 6 M/A vs fluence

Figure 6 shows another characteristic of the MSE. At lower fluences matrix suppression is observed for appropriately high analyte concentrations. the curve for the lower analyte concentration serves to show the position of the MALDI threshold. Above 11 mJ/cm^2 ions are generated in both cases, but at an analyte concentration of 0.025, sufficient analyte is present to react with all matrix ions and the M/A ion ratio is zero. As the fluence is increased, more and more matrix ions are created until they exceed the amount of analyte available, also at [A]=0.025. The reaction becomes reagent limited, and the M/A ratio increases above zero.

This behavior is observed experimentally, as shown in Fig. 5 of ref. 8. For valinomycin (MW=1110 Da) at [A]=0.1 in DHB, matrix suppression was observed for

laser fluences below 60-75 mJ/cm^2 (the fluence uncertainty is due spot size measurement and spatial inhomogeneity). For valinomycin at [A]=0.1 the model predicts matrix suppression (M/A ion ratio <1%) below 53-65 mJ/cm^2, depending on the reaction ΔG which is assumed (-50 to -150 kJ/mol, respectively). The agreement between calculation and experiment is considered to be very good.

Two Analytes, (Analyte Suppression Effects)

It has been shown that one analyte can completely suppress another, even when the two ions are of different types (e.g. protonated and sodiated).[4] Some effort may required to find the appropriate M:A:B concentration ratios necessary for such a full Analyte Suppression Effect (ASE), but incomplete analyte suppression effects are believed to be common. For example it is very rare that all peptides resulting from the enzymatic digestion of a protein are observed in a MALDI spectrum. A few peptides are usually dominant, and these often are the most basic. Given the usual measurement conditions, this pattern is consistent with competition for protons via secondary reactions in the plume.

FIG 7 synthetic spectra

Analyte suppression is predicted by the present model. It is a function of the total matrix:analyte ratio, M:(A+B) and of the ratio between analytes, A:B. As for the matrix suppression effect with one analyte, there must be enough total analyte present to substantially deplete the primary ions. The ASE is therefore generally accompanied by matrix suppression.

When the two analytes are present in equal amounts, relative suppression effects are weak, even if the differences in charge transfer ΔG are significant (unless one ΔG is very small). However, concentration inequalities are found to be magnified. The effect is present whether analytes react with each other or not, but is somewhat stronger if they do. Since matrix is normally present in much greater quantities than either analyte, even a very energetic A´B reaction is unable to have a large effect. Partial analyte suppression is therefore mostly due to differential matrix ion depletion. When full ASE appears, the concentrations are generally high enough that analyte-analyte reactions can contribute significantly.

As seen in Fig. 7, the ASE appears when a moderate excess of the thermodynamically favored analyte is present. To compare quantitatively with experiment, in Fig. 2 of ref. 4, substance P suppressed gramicidin S (ion signal ratio

40:1) in DHB matrix, at concentration ratios of DHB:P:gramicidin of 2000:2:1. The model predicts the same analyte ion ratio at 2000:6:1, nearly the same. At 2000:2:1 the P:gramicidin ion ratio is predicted to be 4, again the model appears to underestimate the rate of matrix-analyte reactions.

Fig. 8 A/B vs concentration ratio

Figure 8 shows the ASE more quantitatively. The effect of the A/B concentration ratio in the sample on the observed ion ratio is stronger than linear, for both strongly (a) and weakly (b) reacting analytes. The effect is similar at other concentrations and laser fluences. The ASE is a straightforward extension of the 2-component MSE (M,A) to a 3 component system (M,A,B), hence the traces of Fig. 5 and Fig. 8 have similar curved approaches to suppression. Curve (b) shows that the MALDI ion ratios will not correspond to the pre-irradiation concentration ratios if one or both analytes is on the right side of Figure 3. The thermodynamically favored analyte will appear more strongly due to its higher reaction rate. The system becomes kinetically rather than thermodynamically limited, as has been observed at low fluences,[6] and is discussed below.

Fig. 9 detailed log-log A/B concentration plots

Figure 9 shows further predicted characteristics of mixed analyte MALDI experiments. As the amount of one analyte in the sample is increased, its relative MALDI intensity vs. the second analyte increases. In the the lower ranges, the concentration dependence lies, for the present model, between linear and quadratic, depending on the characteristics of the analytes involved. At higher concentrations, deviations from the initial behavior are observed. These are smallest when the analyte which most strongly reacts with matrix is more abundant in the sample, see trace (b). When the less reactive analyte is more abundant, as in trace (c), deviations can be larger. A very significant effect appears for analytes of widely differing MW, as seen in trace (a). Even for equally strongly reactive analytes, the concentration curve changes shape dramatically as heavy analyte is added. Since it is more reactive due to the MW effect described above for the MSE, it begins to dominate its smaller reaction partner. Note that Fig. 9 does not include experimental MW-dependent detection efficiency effects, which will always skew the observed ion ratios toward the lighter component.[29-31]

The deviations from the linearity in Figs. 8 & 9 are a composite of two fundamental effects. First is the thermodynamic competition for charge. As noted above, the analyte which reacts most favorably with matrix is expected to generate the strongest ion signal. This is the thermodynamic control model which has been successful in explaining many MALDI effects.[4-6] Second is the kinetic limitation on the extent of reaction by the expansion of the plume. As the plume becomes less dense, the reaction rates slow to the point that they do not reach completion before the collision free regime is reached.[6] The model then predicts a signal ratio which is sensitive to the relative rates of plume dilution and charge transfer reactions. This is illustrated in Fig 9 (d), which is equivalent to (c) except that an increased gas-phase diffusion rate in the plume was assumed. This speeds the charge transfer reactions, and hence moves the ion signal ratio closer to thermodynamic equilibrium. The curve therefore becomes more linear.

Comparison of curves (c) and (d) reinforces the conclusion from the earlier matrix-only model that the plume expansion characteristics are a key aspect of MALDI. Both in that work and here there are indications that the present molecular beam approximation is indeed only an approximation of the true MALDI situation. Currently it appears that the plume is calculated to be too fast initially and too slow further downstream. This limitation must be kept in mind when evaluating the results presented here, and is under further study by other means.

With the above caveats, Figs. 8 and 9 suggest that calibration curves for quantitation with MALDI need to be generated with care. Unless the amounts of interfering substances do not change substantially between samples, the curves may unexpectedly change slope or shape. Extrapolation outside the high end of a calibrated range may also be dangerous.

Fig. 10 A/B vs fluence

To avoid nonlinearities or other complications as seen in Figs. 8 & 9, it might be hoped that a representative A/B ratio could be obtained if an excess of matrix ions were available. As Fig. 10 shows, the desired improvement does not appear likely for useful fluences. In spite of equal analyte amounts, the A/B ion ratio does reach the desired value of 1 at higher fluences. Even at more than 4 times the threshold fluence (11.5 mJ/cm^2), the ratio is still above 1.5. In most MALDI instruments, high fluences such as these can significantly degrade resolution and so are impractical. In

external source instruments this is a not a consideration, which may prove to be an advantage for quantitative applications.

These results lead to some guidelines for practical analysis of mixtures. To the extent compatible with the required sensitivity, a larger matrix : total analyte ratio is better. Higher laser power is also helpful, by providing more primary ions for all analytes. Where possible, large differences in concentration between analytes should be avoided. When using internal standards, they should have similar charge transfer thermodynamics compared to the analytes, and they should be present in similar amounts. In the favorable cases, similar quantities of thermodynamically similar analytes should be amenable to quantitation.

Conclusions

The quantitative rate equation model for UV-MALDI has been extended to include one or more analytes. Using a straightforward model for secondary matrix-analyte and analyte-analyte ion-molecule charge transfer reaction rates, it was possible to achieve this extension without ftting of parameters. The model makes no assumptions about the nature of the ions involved (polarity, cation adduct, etc.), but was applied specifically to the case of proton transfer secondary reactions.

This model was found to be highly successful in reproducing and explaining a variety of known UV-MALDI characteristics. General features include the wide utility of MALDI, which is a result of extensive secondary reactions, except at small ΔG. The relative sensitivity of MALDI for different analytes, such as proteins and peptides vs. synthetic polymers is also explained. Proton transfer secondary reactions with the former are highly exoergic and fast, while cationization reactions of polymers are weakly exoergic and slow.

Certain specific MALDI effects are quantitatively or semi-quantitatively reproduced. Particular success was achieved for the time-delayed two-pulse analyte ion generation curves. This experiment is an important test because it probes both short and long time scales.

Also very important are the model predictions for the matrix and analyte suppression effects. These remarkable phenomena are reproduced with considerable fidelity. In the case of the matrix suppression effect, the concentration, molecular weight and fluence dependencies are all at least semi-quantitatively correct. For the analyte suppression effect, the model correctly shows that the analyte which reacts most energetically with primary matrix ions is strongly favored when in excess.

The model provides several insights that can help to understand and assist with quantitation and analysis of mixtures: Direct and indirect analyte-analyte interactions can lead to nonlinear concentration-dependent intensity effects, but the details are sensitive to the plume characteristics. These effects are minimized when analytes are present in similar amounts. Analyte-analyte effects are also minimized when both react strongly with primary matrix ions and when they do not differ too greatly in molecular weight. Finally, analyte-analyte effects distort signal ratios less if more primary ions are available, such as at higher laser fluences.

Literature Cited

(1) Knochenmuss, R. *J. Mass Spectrom.* **2002**, *37*, 867-877.

(2) Lüdemann, H.-C.; Redmond, R. W.; Hillenkamp, F. *Rapid Comm. Mass Spectrom.* **2002**, *16*, 1287-1294.

(3) Knochenmuss, R.; Vertes, A. *J. Phys. Chem. B* **2000**, *104*, 5406-5410.

(4) Knochenmuss, R.; Stortelder, A.; Breuker, K.; Zenobi, R. *J. Mass Spectrom.* **2000**, *35*, 1237-1245.

(5) Knochenmuss, R.; Zenobi, R. *Chem. Rev.* **2002**, *103*, 441-452.

(6) Breuker, K.; Knochenmuss, R.; Zhang, J.; Stortelder, A.; Zenobi, R. *Int. J. Mass Spectrom.* **2003**, *226*, 211-222.

(7) Knochenmuss, R.; Karbach, V.; Wiesli, U.; Breuker, K.; Zenobi, R. *Rapid Commun. Mass Spectrom.* **1998**, *12*, 529 - 534.

(8) Knochenmuss, R.; Dubois, F.; Dale, M. J.; Zenobi, R. *Rapid Commun. Mass Spectrom.* **1996**, *10*, 871-877.

(9) Karas, M.; Glückmann, M.; Schäfer, J. *J. Mass Spectrom.* **2000**, *35*, 1-12.

(10) Krüger, R.; Pfenninger, A.; Fournier, I.; Glückmann, M.; Karas, M. *Anal. Chem.* **2001**, *73*.

(11) Breuker, K. Doctoral Thesis, Eidgenössische Technische Hochschule, 1999.

(12) Breuker, K.; Knochenmuss, R.; Zenobi, R. *Int. J. Mass Spectrom.* **1999**, *184*, 25.

(13) Kinsel, G.; Knochenmuss, R.; Setz, P.; Land, C. M.; Goh, S.-K.; Archibong, E. F.; Hardesty, J. H.; Marynik, D. *J. Mass Spectrom.* **2002**, *37*, 1131-1140.

(14) Land, C. M.; Kinsel, G. R. *J. Am. Soc. Mass Spectrom.* **2001**, *12*, 726-731.

(15) Land, C. M.; Kinsel, G. R. *J. Am. Soc. Mass. Spectrom.* **1998**, *9*, 1060-1067.

(16) Allwood, D. A.; Dyer, P. E.; Dreyfus, R. W.; Perera, I. K. *Appl. Surf. Sci.* **1997**, *110*, 616-620.

(17) Allwood, D. A.; Dyer, P. E.; Dreyfus, R. W. *Rapid Commun. Mass Spectrom.* **1997**, *11*, 499-503.

(18) Karbach, V.; Knochenmuss, R. *Rapid Commun. Mass Spectrom.* **1998**, *12*, 968-974.

(19) Yingling, Y. G.; Zhigilei, L. V.; Garrison, B. J.; Koubenakis, A.; Labrakis, J.; Georgiou, S. *Appl. Phys. Lett.* **2001**, *78*, 1631-1633.

(20) Zhigilei, L. V.; Garrison, B. J. *Appl. Phys. Lett.* **1999**, *74*, 1341-1343.

(21) Zhigilei, L. V.; Garrison, B. J. *Appl. Phys. A* **1999**, *69*, S75-S80.

(22) Zhigilei, L. V.; Kodali, P. B. S.; Garrison, B. J. *Chem. Phys. Lett.* **1997**, *276*, 269-273.

(23) Valentine, S. J.; Counterman, A. E.; Clemmer, D. E. *J. Am. Soc. Mass Spectrom.* **1999**, *10*, 1188-1211.

(24) Agmon, N.; Levine, R. D. *Israel J. Chem.* **1980**, *19*, 330.

(25) Agmon, N. *Int. J. Chem. Kin.* **1981**, *13*, 333.
(26) Kinsel, G. R.; Edmondson, R. D.; Russell, D. H. *J. Mass Spectrom.* **1997**, *32*, 714-722.
(27) Fournier, I.; Brunot, A.; Tabet, J.-C.; Bolbach, G. *Int. J. Mass Spectrom.* **2002**, *213*, 203-215.
(28) Livadaris, V.; Blais, J.-C.; Tabet, J.-C. *Eur. J. Mass Spectrom.* **2000**, *6*, 409-413.
(29) Geno, P. W.; Macfarlane, R. D. *Int. J. Chem. Mass Spectrom.* **1989**, *92*, 195.
(30) Brunelle, A.; Chaurand, P.; Della Negra, S.; LeBeyec, Y. *Rapid Comm. Mass Spectrom.* **1997**, *11*, 353.
(31) Dubois, F.; Knochenmuss, R.; Zenobi, R.; Brunelle, A.; Deprun, C.; LeBeyec, Y. *Rapid Comm. Mass Spectrom.* **1999**, *13*, 786.
(32) Carr, S. R.; Cassidy, C. J. *J. Am. Soc. Mass Spectrom.* **1996**, *7*, 1203-1210.
(33) Carr, S. R.; Cassady, C. J. *J. Mass Spectrom.* **1997**, *32*, 959-967.
(34) Zhang, X.; Cassady, C. J. *J. Am. Soc. Mass Spectrom.* **1996**, *7*, 1211-1218.
(35) Gross, D. S.; Williams, E. R. *J. Amer. Chem. Soc.* **1996**, *118*, 202-204.
(36) Harrison, A. G. *Mass Spectrom. Rev.* **1997**, *16*, 201 - 217.
(37) Steenvoorden, R. J. J. M.; Breuker, K.; Zenobi, R. *Eur. Mass Spectrom.* **1997**, *3*, 339-346.
(38) Burton, R. D.; Watson, C. H.; Eyler, J. R.; Lang, G. L.; Powell, D. H.; Avery, M. Y. *Rapid Commun. Mass Spectrom.* **1997**, *11*, 443-446.
(39) Mormann, M.; Bashir, S. M.; Derrick, P. J.; Kuck, D. *J. Am. Soc. Mass Spectrom.* **2000**, *11*, 544-552.
(40) Klassen, J. S.; Anderson, S. G.; Blades, A. T.; Kebarle, P. *J. Phys. Chem.* **1996**, *100*, 14218-14227.
(41) Zhang, J.; Knochenmuss, R.; Stevenson, E.; Zenobi, R. *J. Mass Spectrom.* **2002**, *213*, 237-250.
(42) Zhang, J.; Ha, T.-K.; Knochenmuss, R.; Zenobi, R. *J. Phys. Chem. A* **2002**, *106*, 6610-6617.
(43) Hoyau, S.; Norrman, K.; McMahon, T. B.; Ohanessian, G. *J. Am. Chem. Soc.* **1999**, *121*, 8864.
(44) Chen, R.; Yalcin, T.; Wallace, W. E.; Guttman, C. M.; Li, L. *J. Am. Soc. Mass Spectrom.* **2001**, *12*, 1186-1192.
(45) Moskovets, E.; Vertes, A. *J. Phys. Chem. B* **2002**, *106*, 3301-3306.

Figures

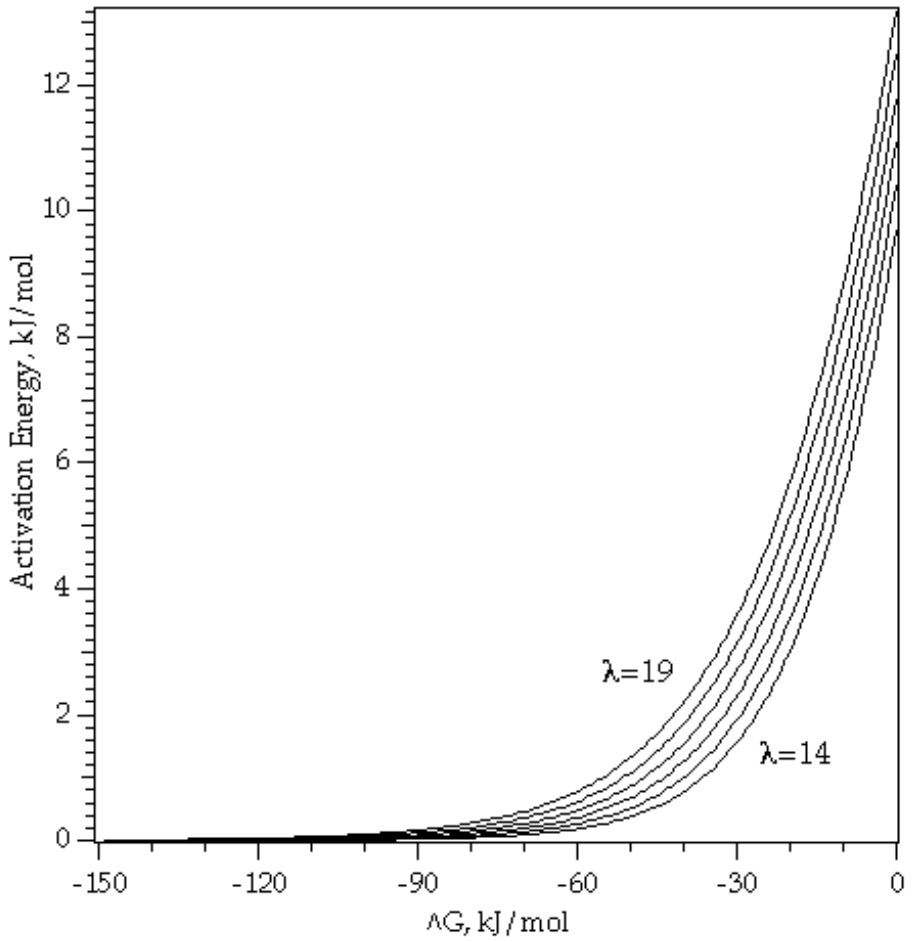

Figure 1. Activation energy from the Agmon-Levine free energy relationship[24,25] vs. ΔG of the proton transfer reaction. Lambda values of 14-19 have been found for gas-phase proton transfers, and are shown. A lambda value of 15 was used for this work, on the basis of studies of MALDI matrix molecules.[11]

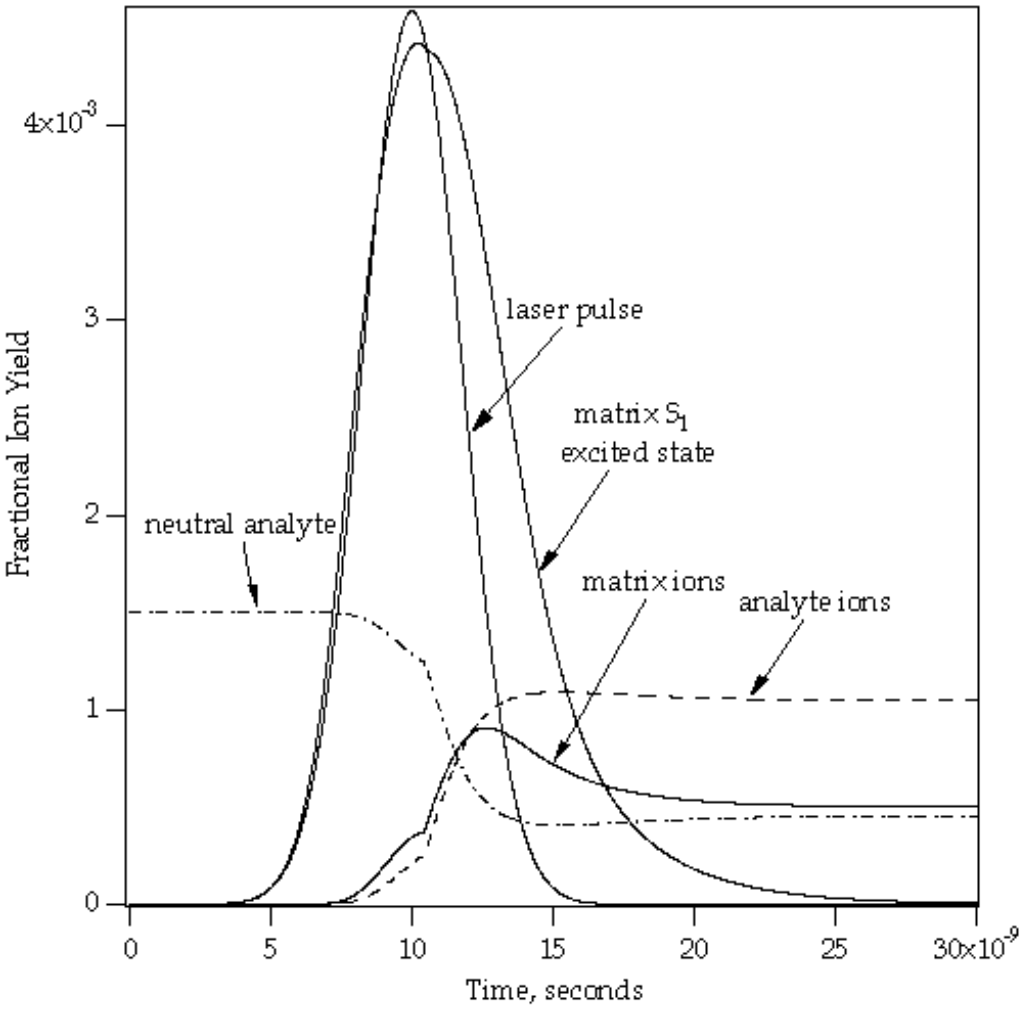

Figure 2. Example results for the MALDI rate equation model including one analyte. Matrix parameters are as in ref. 1, corresponding to 2,5 dihydroxybenzoic acid (DHB). The laser wavelength was 355 nm. The matrix-to-analyte reaction exoergicity was -150 kJ/mol, typical for proton transfer from $(DHB)H^+$ to small peptides. The laser fluence was 24 mJ/cm^2, and the concentration of 1 kDa analyte 0.015 mol/mol. At about 11 ns, the sample reaches the sublimation temperature of 450 K and begins to expand, enabling primary and secondary ion generation to accelerate, before slowing again as the plume expands.

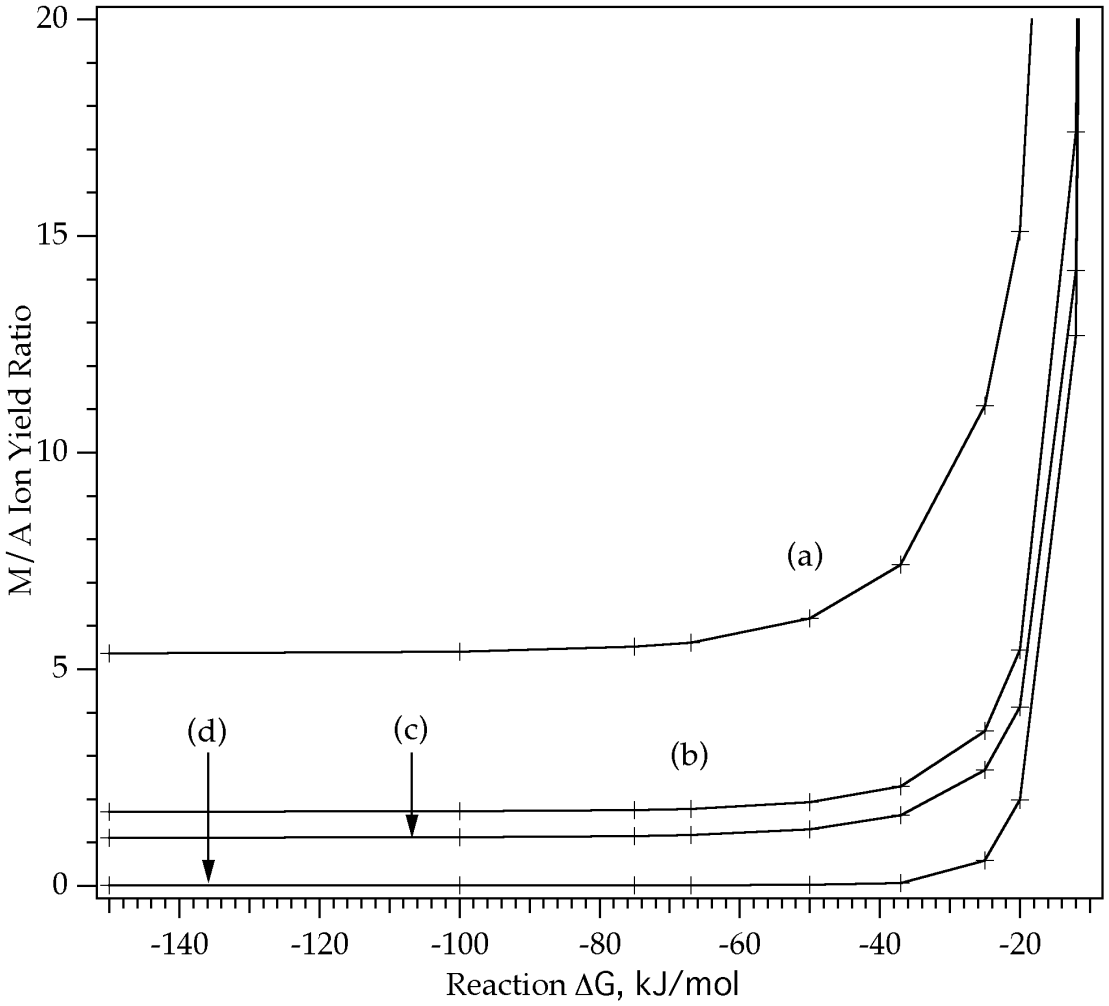

Figure 3. Matrix-to-analyte ion yield ratio vs. driving force of the secondary reaction. For most of the MALDI-relevant range shown, the reaction is efficient. Only at $\Delta G > -40$ kJ/mol does it slow sufficiently to leave large amounts of primary matrix ion unreacted, and increase the M/A ratio. (a) Analyte concentration [A]=0.002, MW=1 kDa, 15 mJ/cm^2. (b) [A]=0.004, MW=1 kDa, 20 mJ/cm^2. (c) [A]=0.004, MW=1 kDa, 15 mJ/cm^2. (d) [A]=0.002, MW=10 kDa, 15 mJ/cm^2.

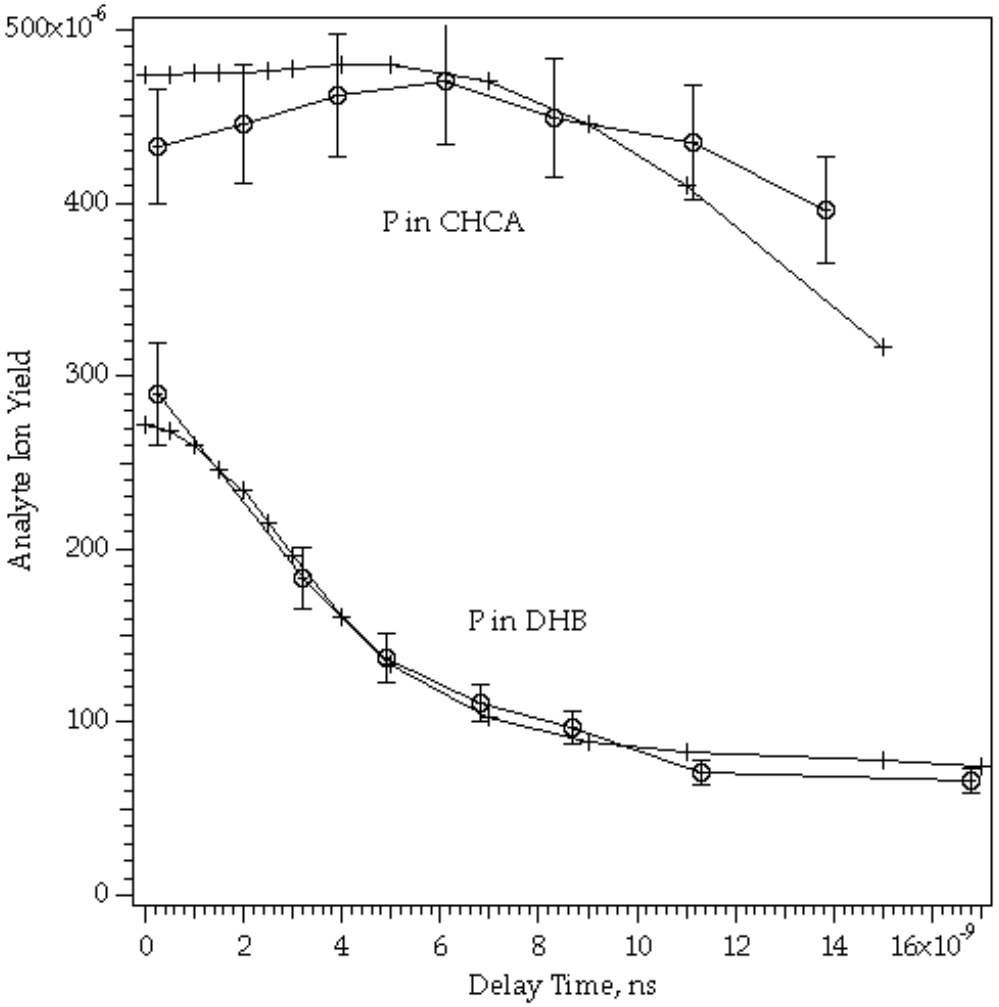

Fig. 4. Time-delayed 2-pulse MALDI data and corresponding calculations using the present model. The ion yield of substance P in DHB or CHCA (a-cyano-4-hydroxycinnamic acid) matrix is plotted vs delay time between two 3 ns nitrogen laser pulses. The data is from ref. 45, and represented by round symbols. For P in DHB, agreement of model and data is excellent.

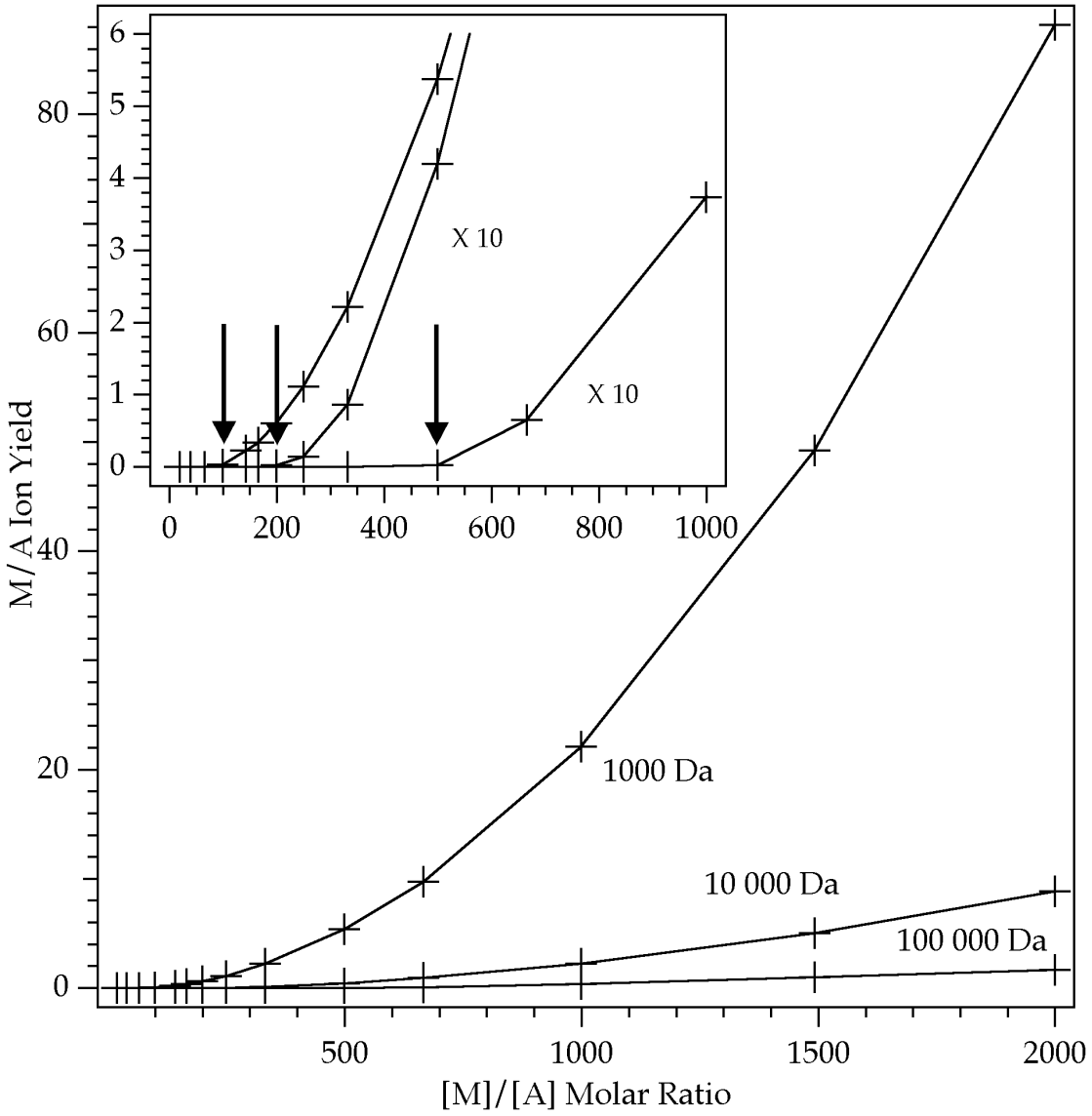

Figure 5. Matrix-to-analyte ion yield ratio vs. the M/A concentration ratio in the sample, for 3 analyte molecular weights. The matrix suppression effect is predicted by the model, as well as the molecular weight dependence of the M/A ratio at which suppression is reached. The nonlinear approach to suppression is also qualitatively similar to that experimentally observed.[7]

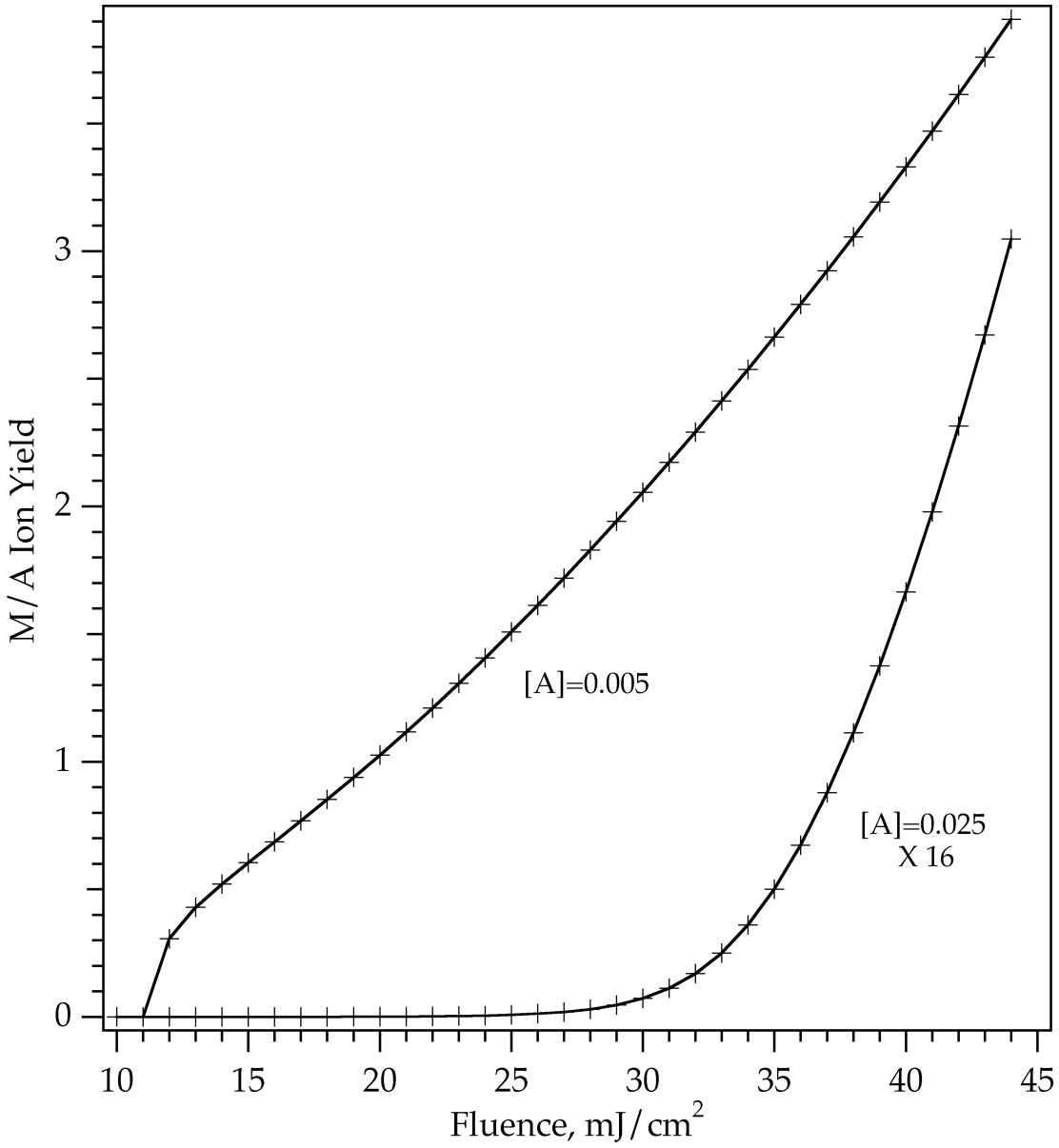

Figure 6. Matrix-to-analyte ion yield ratio vs. the laser fluence, for two analyte concentrations. The lower concentration makes the MALDI threshold at 12 mJ/cm^2 apparent. From threshold to 25 mJ/cm^2 the higher concentration sample exhibits matrix suppression (M/A ion ratio =0). As the fluence is increased further, more matrix ions are generated than consumed in secondary reactions, so the M/A ion ratio becomes nonzero. This is as observed experimentally.[8] Analyte MW=1kDa, ΔG=-150 kJ/mol.

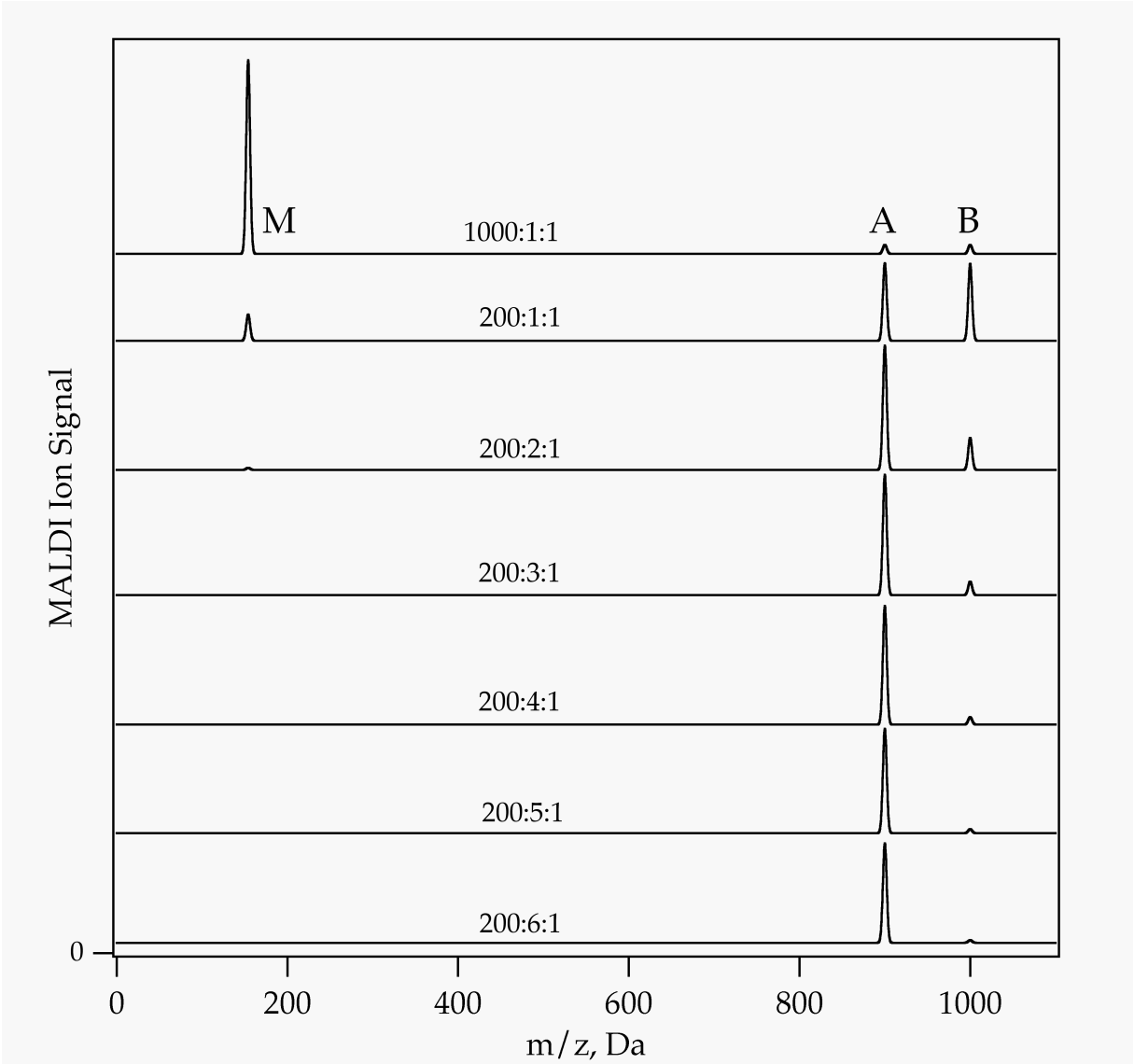

Figure 7. Simulated MALDI mass spectra of a sample containing matrix M and two analytes, A & B, vs. mixing ratios in the sample. Both matrix suppression and suppression of B by A are observed. The spectra are all plotted on the same scale, relative intensities can be compared. The matrix-analyte secondary reactions were characterized by: $\Delta G(A)=-150$ kJ/mol; $\Delta G(B)=-100$ kJ/mol. The $A + B^+ \rightarrow A^+ + B$ reaction therefore had $\Delta G=-50$ kJ/mol. See the text for further discussion.

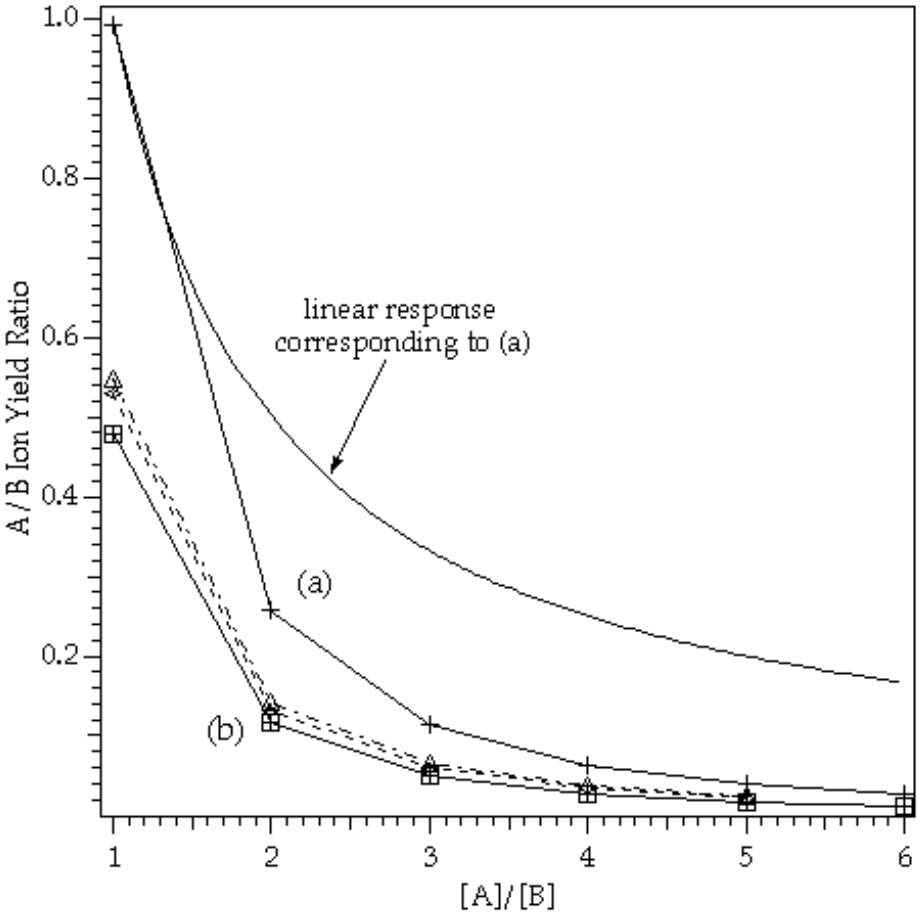

Figure 8. Dependence of the A/B MALDI ion yield ratio on the A/B ratio in the sample prior to laser irradiation. The concentration of B was 0.005, the concentration of A was varied to change A/B. (a) ΔG(A)=-150 kJ/mol; ΔG(B)=-100 kJ/mol. (b) ΔG(A)=-75 kJ/mol; ΔG(B)=-50 kJ/mol. Also shown is the signal ratio expected if A and B ion signals were linearly correlated with concentration in the sample.

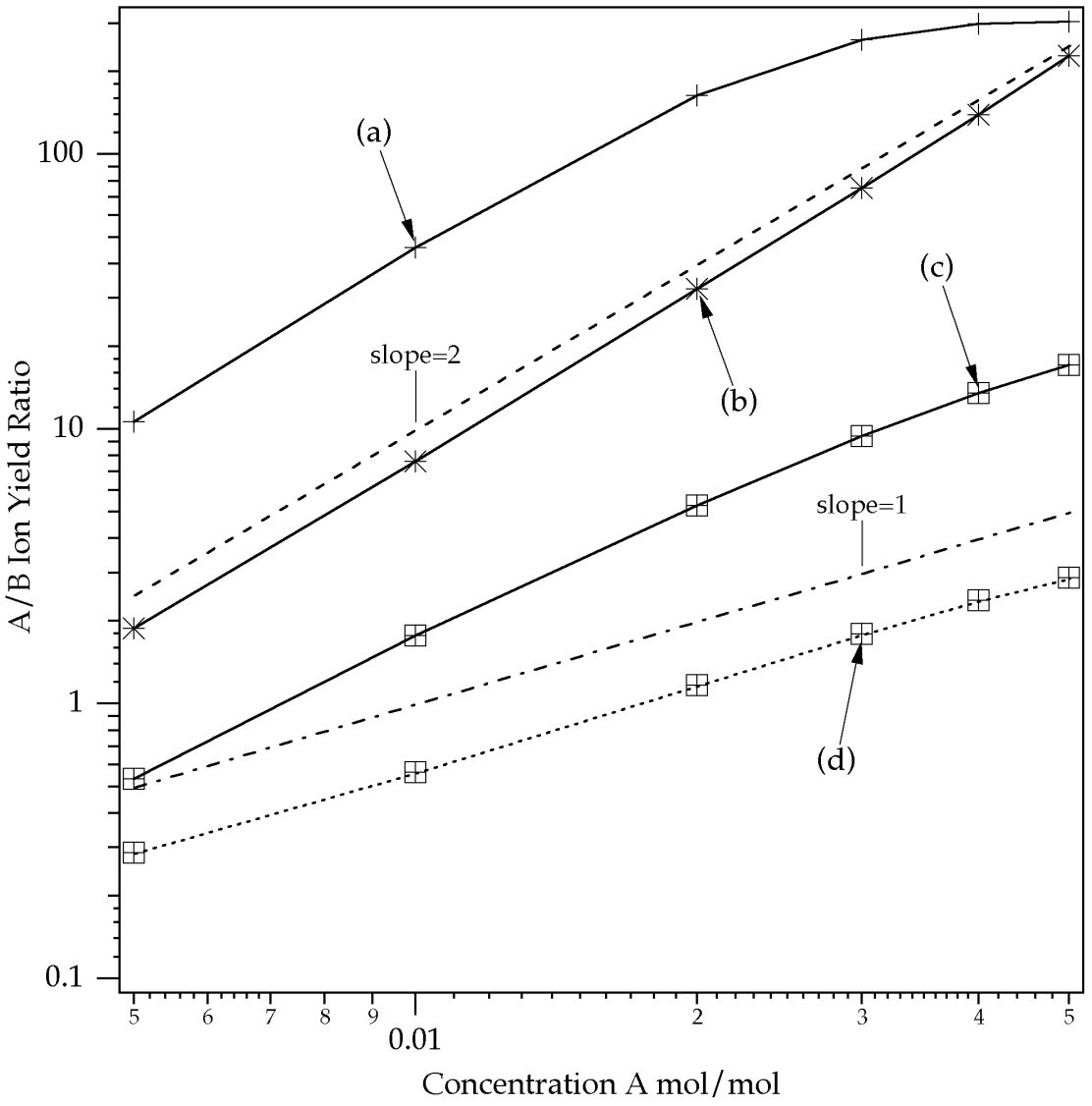

Figure 9. Dependence of the A/B MALDI ion yield ratio on the [A]/[B] ratio in the sample, over a wide range. Unless otherwise noted, [B]=0.005, MW(A)=MW(B)=1 kDa. The dashed lines show linear and quadratic dependencies for comparison. (a) $\Delta G(A)$ = -100, $\Delta G(B)$=-100 kJ/mol, MW(A)=10 kDa. (b) $\Delta G(A)$=-50, $\Delta G(B)$=-25 kJ/mol. (c) $\Delta G(A)$=-25, $\Delta G(B)$=-50 kJ/mol. (d) as in (c), but with increased reaction rate in the plume (see text).

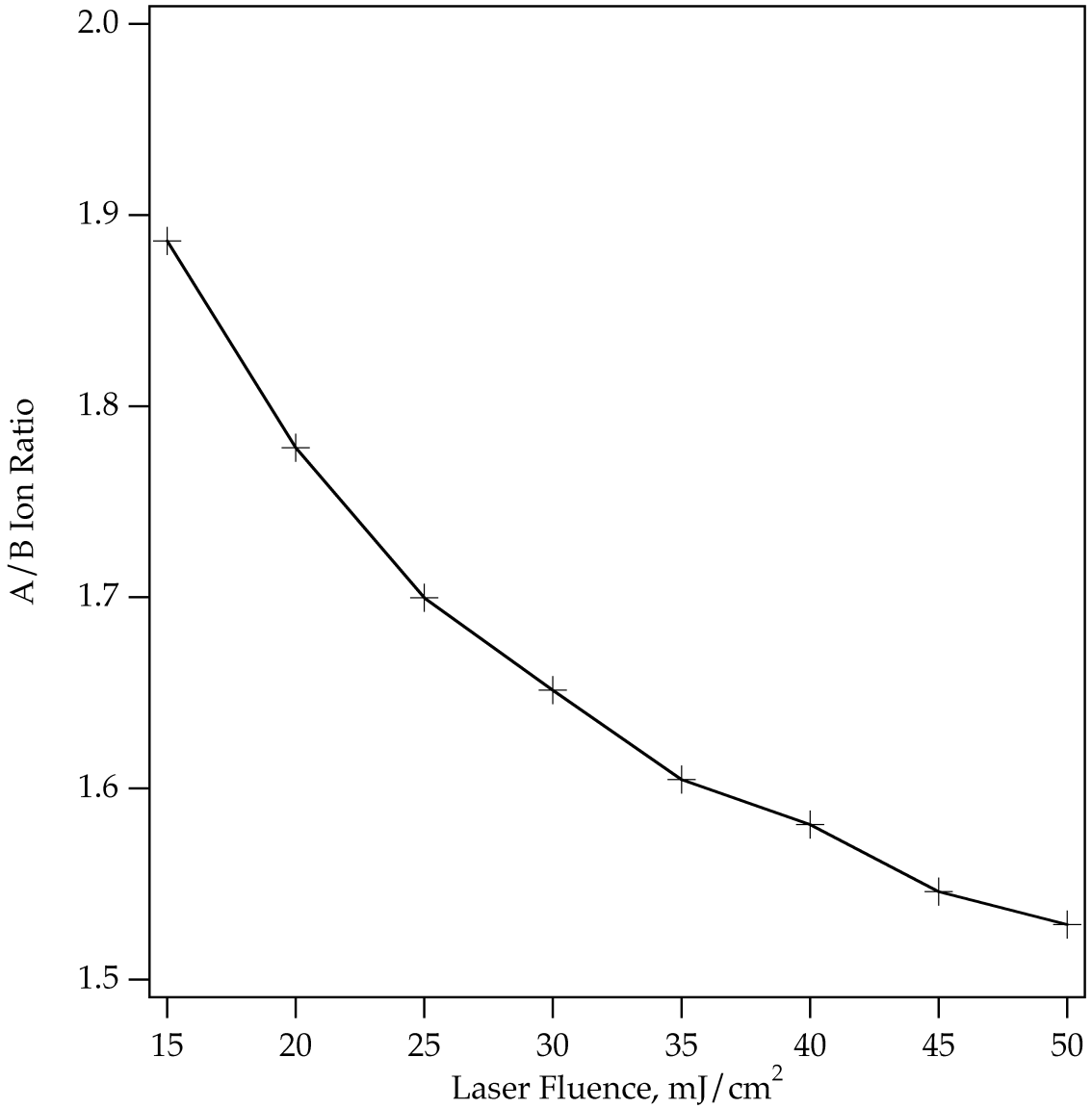

Figure 10. Dependence of the A/B MALDI ion yield ratio on laser fluence, for a sample containing equal amounts of A and B. Analyte A reacts more strongly with primary matrix ions: $\Delta G(A)$=-50 kJ/mol; $\Delta G(B)$=-25 kJ/mol. As the amount of matrix ions increases with laser fluence, the A/B ion ratio drops toward the desired [A]/[B] ratio of 1, but does not drop below 1.5 at >4 times the threshold fluence (12 mJ/cm^2).